RSC Advances

PAPER

View Article Online
View Journal | View Issue

Cite this: *RSC Adv.*, 2015, **5**, 10560

Synthesis of dimethyl carbonate (DMC) based biodegradable nitrogen mustard ionic carbonate (NMIC) nanoparticles†

P. Thyriyalakshmi and K. V. Radha*

Chitosan-nitrogen mustard ionic carbonate nanoparticles (C-NMIC-Nps) were fabricated for the first time by an ionotropic gelation method. The preparation of C-NMIC-Nps involved four steps. In the first step, green reagent dimethyl carbonate (DMC) reacted with 2-dimethylethanolamine (DMEA) to form bis-(2-dimethyl amino-ethyl)carbonate (DAEC). In the second step, DAEC underwent cationization with (1-chloro-2,3 epoxy)propane to form NMIC with a stable carbonate backbone having a greater number of sorption sites. Later, NMIC was successfully cross linked with chitosan to form C-NMIC, which was later on used to form C-NMIC nanoparticles (C-NMIC-Nps) by ionotropic gelation. The chemical structure of NMIC and C-NMIC was identified by proton nuclear magnetic resonance (^{1}H-NMR), ^{13}C nuclear magnetic resonance (^{13}C-NMR) spectroscopy and elemental analysis. The spherical shaped, smooth and uniform distribution of the C-NMIC-Nps was observed by scanning electron microscopy (SEM) and high resolution transmission electron microscopy (HRTEM). The average particle size distribution of the C-NMIC-Nps was found to be 14.4 ± 3.1 nm as observed using a particle size analyzer. The functional groups of DAEC, NMIC and C-NMIC were identified by Fourier transform infrared spectroscopy (FTIR). The conversion of the crystalline nature of chitosan to the amorphous state in C-NMIC-Nps was studied by X-ray diffraction (XRD). The thermal stability of the C-NMIC-Nps was confirmed by thermo gravimetric analysis (TGA). The good cell viability of C-NMIC-Nps was assessed by *in vitro* MTT assay using VERO cell lines. Overall, the results suggested that C-NMIC-Nps had been prepared successfully. The prepared C-NMIC-Nps will act as a nano carrier of growth factors for wound healing application.

Received 28th October 2014
Accepted 6th January 2015

DOI: 10.1039/c4ra13290d

www.rsc.org/advances

1. Introduction

In modern polymer science a wide range of materials, such as natural or synthetic polymers, lipids, surfactants and dendrimers have been employed as drug carriers. Among these, polysaccharides have received increasing attention because of their outstanding physical and biological properties.[1]

In recent years, naturally occurring carbohydrate based biopolymers chitin and chitosan have gained impetus because of their excellent biocompatibility.[2] Since, chitin and chitosan exist with some unique properties like biodegradability and bioactivity, and have a variety of potential applications in biomedical and biotechnological fields. Chitosan is more efficient than chitin in terms of adsorption capacity due to the presence of large number of free amino groups on the chitosan chain.[3]

Chitosan is a poly cationic biopolymer obtained mainly by deacetylation of chitin, which is the second most abundant natural polymer after cellulose. It is a linear co-polymer of β-(1,4)-2-acetamido-2-deoxy-β-D-glucose and β-(1,4)-2-amine-2-deoxy-β-D-glucose.[4] Chitosan has both reactive amino and hydroxyl groups, that can chemically alter its properties, under mild conditions. It is generally regarded as biocompatible, biodegradable and nontoxic biomaterial. Chitosan has been proved to have antifungal property. It is an attractive candidate for treating wounds by acting as a haemostat and initiates fibroblast proliferation at the wound site.[5]

Chitosan shows high crystallinity and high degree of hydrogen bonding leading to poor solubility in water and common organic solvents.[6] In recent years, there has been a growing interest in the modification of chitosan and its utilization as diversified agent in pharmaceutical, waste water treatment, cosmetics, drug delivery, heavy metal chelation, heterogeneous catalysis and many other applications.[7] Ionic or covalent crosslinking between the polymeric chains plays a vital role in the formation of nanoparticles.[8]

Cross linkers are molecules with two reactive functional groups that allow the formation of bridges between the polymeric chains.[9] Cross linked chitosan is very stable and maintain their strength even in acidic and basic solutions. It leads to the change in crystalline nature of chitosan and enhance sorption properties.[10]

Bio-Products Laboratory, Department of Chemical Engineering, A.C. Tech, Anna University, Chennai-25, Tamil Nadu, India. E-mail: radhavel@yahoo.com; Tel: +91-44-22359124

† Electronic supplementary information (ESI) available. See DOI: 10.1039/c4ra13290d

Chitosan is able to form nanoparticles which were harvested spontaneously under mild acidic conditions in contact with negatively charged sodium tripolyphosphate (TPP) ions by ionotropic gelation method. This type of ionic cross linking of chitosan is usually a typical non-covalent interaction, which is reversible and this may avoid the potential toxicity of the reagent.[11]

The chemical modification of chitosan affords a wide range of derivatives such as quaternary chitosan, carboxy alkyl chitosan, thiolated chitosan, sugar bearing chitosan, bile acid modified chitosan and cyclodextrin-linked chitosan. The derivatives of chitosan impart amphiphilicity, which is an important characteristic for the formation of self-assembled nanoparticles, potentially suited for biomedical applications.[12]

Among the several chitosan derivatives, chitosan with cationic moieties has been prepared by quaternization of the amino group or by grafting small molecules or polymer chains on to chitosan backbone. By introducing the cationic nature of chitosan several drug conjugate approaches have been developed towards therapeutic applications.[13]

Recently, chitosan acetate with both hemostatic and antimicrobial properties has been used for wound healing application.[14] A good wound healing material should maintain a moist environment but allows the drainage of wound exudate and prevents infection at the wound site. Hydroxypropyl chitosan is used as a delivery vehicle for fibroblast growth factor that accelerates wound healing.[15] Biocompatible and water soluble carboxymethyl chitosan nanoparticles has been studied for delivery of antibiotics.[16]

Nowadays sulfur and nitrogen (half-) mustards are extensively employed in inorganic synthesis, organic synthesis and in the preparation of numerous pharmaceutical intermediates. These compounds are toxic and the toxicity is strictly related to their highly reactive chlorine atom. The replacement of chlorine atom by a carbonate moiety with DMC[17] an eco-friendly, biodegradable and nontoxic reagent resulted in sulfur and nitrogen half mustard carbonate analogues. These analogues showed to maintain the chemical behaviour of the parent chlorine compounds, while losing their toxic properties.[18] Thus, the current study mainly focussed on the synthesis of nitrogen mustard ionic carbonate (NMIC).

The objective of the study is to develop a novel, facile route for the preparation of biodegradable chitosan-nitrogen mustard ionic carbonate nanoparticles (C-NMIC-Nps) with a stable carbonate backbone that offers a great promise as wound healing platform. In the present work, a novel DMC based NMIC was synthesized and cross linked with chitosan to produce C-NMIC. Herein, DMC provides a stable carbonate moiety to the newly synthesized NMIC. Then, a simple ionotropic gelation method was used to prepare the C-NMIC-Nps. The cationic and the hydrophilic property of NMIC, would enhanced the sorption properties of chitosan, making C-NMIC-Nps a promising material in therapeutics.

The synthesized NMIC, and the prepared C-NMIC and C-NMIC-Nps were characterized by various methods namely FTIR, ^{1}H-NMR, ^{13}C-NMR, elemental analysis, SEM, HR-TEM, particle size analysis, XRD and TGA. The biocompatibility of C-NMIC-Nps was assessed by *in vitro* cytotoxicity test (MTT assay).

2. Experimental methods

2.1 Materials

Analytical grade dimethyl carbonate (DMC), 2-dimethylethanolamine (DMEA), triethyl amine (TEA) and epichlorohydrin were purchased from Sigma Aldrich. Chitosan of low molecular weight (85% deacetylation) with viscosity >200 cps, sodium tripolyphosphate (TPP) with 85% purity and MTT [3-(4,5-dimethylthiazol-2-yl)-2,5-diphenyl tetrazolium bromide] with 98% purity were also obtained from Sigma Aldrich. All other reagents were analytical grades and were used without any further purification. Milli-Q grade (resistivity 18.2 MΩ cm^{-1}) water was used in all the experiments.

2.2 Characterization of DAEC, NMIC, C-NMIC and C-NMIC-Nps

FTIR spectra of all the samples were recorded using Alpha Bruker spectrophotometer in attenuated total reflectance (ATR) mode in the range of 4000–400 cm^{-1}. ^{1}H-NMR and ^{13}C-NMR spectra of the samples were recorded on a Bruker D8 advance 500 spectrometer at 25 °C using D_2O and D_2O/CF_3COOD as solvents. Mass spectra were recorded on a (EI) JEOL JMS-AX 500. Elemental analysis was performed on a Heraeus CHN-O-Rapid analyser. XRD Patterns were done with a Bruker D8 Advance XRD machine using Cu-Kα (λ = 1.54 Å) source. The layer spacing of the samples was calculated according to the Bragg's equation. The diffraction angles 2θ were set between 2° and 75° incremented with a scanning angle of 1° min^{-1}.

Thermal stability was examined by the TGA of TA Perkin Elmer instrument at a heating rate of 20 K min^{-1} in the temperature range between 30–700 °C under nitrogen atmosphere. The average particle size distribution was determined using dynamic light scattering (DLS) analyzer with a Malvern Zetasizer Nano-S. For SEM analysis, the particles were sputter-coated with gold film using a sputter coater and imaged under SEM (TESCAN-VEGA3 SBU). For HRTEM studies of the nanoparticles, 5 μL of the sample was coated on a carbon-coated copper HRTEM grid, which was subsequently air dried and was analysed by a high resolution HRTEM (JEM 2100, Jeol, Peabody, MA, USA) operating at a high voltage of 200 keV. The selected area electron diffraction (SAED) pattern of the C-NMIC was also recorded using the same instrument.

2.3 Preparation of NMIC and C-NMIC

2.3.1 Synthesis of bis-(2-dimethyl amino-ethyl)carbonate (DAEC). 0.1 M (8.4 mL) of DMC was allowed to reflux with 0.2 M (27 mL) of DMEA in the presence of TEA (13.9 mL) base as a catalyst at 86–88 °C for about 24 h. The crude compound was subjected to fractional distillation under vacuum at 60 °C. The yield of the coloured orange product was found to be 47.3%. FTIR: ν_{max}/cm^{-1} 1652 (ester C=O str), 1496 (N–CH_3 assy def), 1386 (CH_2 def CH_2–O), 1254 (ester C–O assy str), 1094 (ester C–O sym str), 864 (C–N str), 660 (CH_2 rock). ^{1}H-NMR (500 MHz, D_2O):

δ_H ppm 3.06 (12H, s, N–CH_3), 3.38 (4H, t, $J = 4.5$, N–CH_2), 3.91–3.95 (4H, m, O–CH_2). ^{13}C-NMR (500 MHz, D_2O): δ_c 54 (N–CH_3), 56 (N–CH_2), 67 (O–CH_2), 161 (C=O). EI-MS (*m*/*z*): 207 (M + 2, 130%).

2.3.2 Synthesis of bis-{2-[(3-chloro-2-hydroxy propyl)-*N*,*N*-dimethyl ammonium chloride]-ethyl}carbonate (CHPDAEC)/(NMIC). DAEC obtained in the first step was mixed with excess amount 2 mL of 1-chloro-2,3-epoxy propane in methanol and stirred at 50 °C for 16 h in the presence of acid catalyst. The crude product NMIC was obtained at 65 °C after fractional distillation under vacuum. Later, the pure product with a yield of 57.9% was subsequently obtained as a brown colour liquid after ether separation in diethyl ether. FTIR: ν_{max}/cm^{-1} 3464 (alcoholic OH str), 1652 (ester C=O), 1386 (CH_2 def CH_2–O), 1336 (CO def of CHOH), 1162 (alcoholic C–O str), 1012 (CH_2 def of CH_2OH), 1254 (ester C–O assy str), 960 (OH def of CHOH), 834 (C–N str), 660 (CH_2 rock), 602 (C–Cl str). ^{1}H-NMR (500 MHz, D_2O): δ_H ppm 3.2 (12H, s, N–CH_3) 3.5–3.67 (8H, m, NCH_2), 3.9–4.1 (4H, m, OCH_2), 4.8–4.9 (2H, m, CH_2–CH–CH_2), 3.4–3.48 (4H, m, CH_2Cl). ^{13}C-NMR (500 MHz, D_2O): δ_c ppm 54 (N–CH_3), 55 (N–CH_2–CH_2) and (O–CH_2), 63 (N–CH_2–CH), 67 (CH_2–CH–OH), 53 (C–Cl), 165 (C=O). EI-MS (*m*/*z*): 391.2 (M^+ − Cl, 100%).

2.3.3 Modification of chitosan with NMIC. 1.6 g of chitosan was being dissolved in 1% acetic acid. The pH of the solution was adjusted to 4 by the addition of 0.1 M Na_2CO_3 solution and kept for continuous stirring. Solution of 0.1 M NMIC in methanol was added drop wise to chitosan. To the resultant mixture, 0.1 M Na_2CO_3 was added until the solution attained the pH 7–8 and stirring was continued for 24 h. The precipitated NMIC was subjected to repeated centrifugation and washed with 1 : 1 CH_3OH/H_2O, till the pH of the solution becomes neutral. The formed C-NMIC was dried in a vacuum oven at 55 °C overnight and stored in a desiccator. FTIR: ν_{max}/cm^{-1} 3280 (OH str and NH str of primary amine), 1642 (C=O str of amide), 1564 (NH bends of amide), 1374 (sym angular deformation of CH_3), 1318 (CO def of CH–OH), 1258 (ester assy C–O str), 1150, 1062, 1030 and 896 (sym str of C–O–C), 822 (C–N str), 798 (OH bend). ^{1}H-NMR (500 MHz, D_2O/CF_3COOD): δ_H ppm 1.3 (br, 3H, s, NHCOCH_3), 2.4–2.5 (br, 4H, d, (NH–CH_2)), 2.9–3.2 (br, 4H, d, (N–CH_2–CH(OH))), 3.3 (br, 12H, s, (N–CH_3)), 3.5–4.9 (br, m, (2H, N–CH_2–CH_2–O), (H1, H2, H3, H4, H5, H6, H6′), (4H, OCH_2), (1H, CHOH)). ^{13}C-NMR (500 MHz, D_2O/CF_3COOD): δ_c ppm 22 (CH_3CO), 52 (N–CH_3), 54 (NH–CH_2), 56 (N–CH_2), 60 (C6), 61 (O–CH_2), 63 (C_2), 67 (CH_2–CH–OH), 73 (C3), 74 (C5), 78 (C4), 105 (C1), 167 (C=O).

2.3.4 Preparation of C-NMIC nanoparticles. To about 0.1% w/v of C-NMIC in aqueous acetic acid, 0.01% w/v TPP was gently dripped and the solution was allowed to stand for 10 min at room temperature to get an opalescent suspension. The resulting nanoparticles were centrifuged at 10 000 rpm for 30 min at 4 °C. The precipitated nanoparticles were once again re-suspended in water, sonicated, centrifuged and freeze dried.

2.4 Cytotoxicity studies

2.4.1 Cell culture. The cytotoxicity of the pure C-NMIC-Nps on VERO cells were assessed by 3-(4,5-dimethylthiazol-2-yl)-2,5-diphenyl-tetrazolium bromide (MTT) assay. The VERO (kidney epithelial from African monkey) cells were grown and maintained in Dulbecco's modified eagle medium (DMEM) containing high glucose and pyruvate, with 10% fetal calf serum (FCS) supplemented with penicillin (120 units per mL), streptomycin (75 mg mL^{-1}), gentamycin (160 mg mL^{-1}) and amphotericin B (3 mg mL^{-1}) at 37 °C in an incubator humidified with 5% CO_2. Confluent cells were harvested by washing in phosphate-buffered solution (PBS), followed by trypsinization for subculture. The cell proliferation and viability were measured by MTT assay to determine the amount of the active mitochondrial enzymes present in the viable cells.

2.4.2 Experimental design for the evaluation of cytotoxicity effects. The cytotoxicity effects of C-NMIC-Nps were assessed using VERO cell lines. The nanoparticles were sterilized by UV treatment before subjecting them to the cell culture procedures. C-NMIC-Nps of various concentration (0.5, 1, 1.5, 2.0 and 2.5 mg mL^{-1}) were placed in the 96 wells of a polystyrene tissue culture plate. The cellular behaviour of the nanoparticles was observed after 12 h, 24 h, 48 h and 72 h respectively. The polystyrene surface (wells without C-NMIC-Nps) was treated as control. In all the culture conditions, the medium was renewed every day and at the end of incubation, the supernatant of each well was replaced with MTT diluted in a serum-free medium. The plates were then incubated at 37 °C for 4 h. After aspirating the MTT solution, DMSO was added to each well, and pipetted up and down to dissolve all of the dark blue crystals of formazan, and then left at room temperature for few minutes. Finally, the absorbance at 570 nm was measured, using the UV spectrophotometer. Experiments were repeated as triplicate per sample. The absorbance of the control group was taken as 100% and the percentage of cell viability was recorded by the following equation.

$$\text{Cell viability } (\%) = \frac{\text{OD (test)} - \text{OD (blank)}}{\text{OD (control)} - \text{OD (blank)}} \times 100\% \quad (1)$$

3. Results and discussion

3.1 Mechanism

DAEC was synthesized by the reaction of DMC with DMAE at 88 °C through $B_{AC}2$ mechanism as given in Scheme 1. When DMEA attacks the carbonyl carbon of DMC, carboxy methylation reaction takes place resulting in the formation of the expected DAEC and by-product methanol.[17] The second step in Scheme 1 represents the synthesis of NMIC by nucleophilic addition reaction. Herein, DAEC in the presence of acid catalyst attack the C_3 carbon of epoxy ring of 1-chloro(2,3 epoxy) propane, resulting in the three member ring opening reaction. Covalent attachment of NMIC to chitosan through *N*-alkylation was shown in Scheme 2. Wherein, *N*-alkylation of chitosan with NMIC takes place through the liberation of HCl at pH 7–8.[19]

The successful attachment of NMIC to chitosan was confirmed by elemental analysis (Table 1). The presence of NMIC in the modified chitosan caused a decrease in the carbon and hydrogen content in the resulting C-NMIC material.

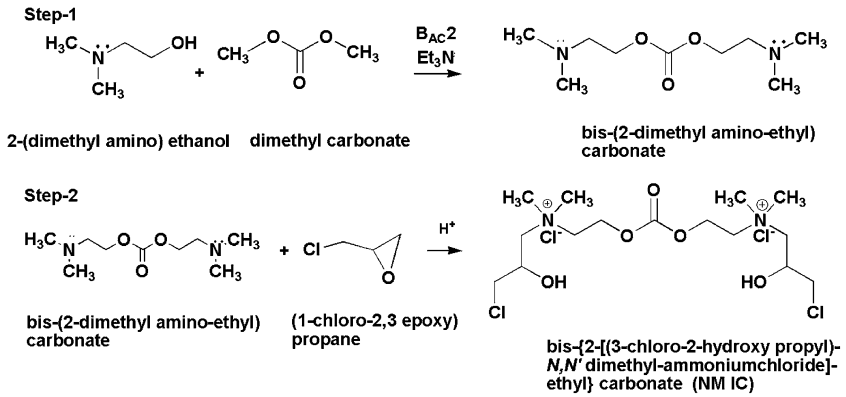

Scheme 1 Formation of DAEC and NMIC.

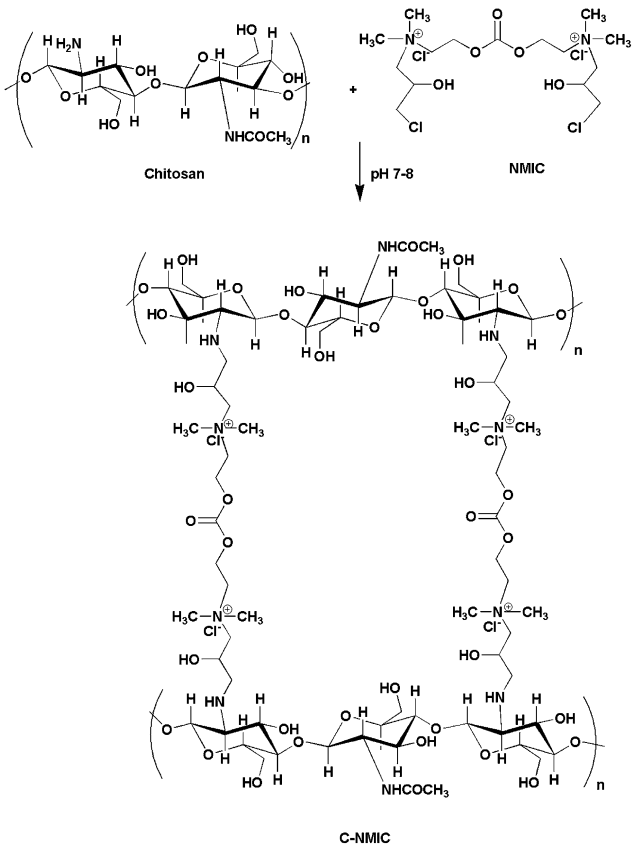

Scheme 2 Schematic structure newly synthesised C-NMIC.

However, the percentage of nitrogen increases with the addition of NMIC to the chitosan sequence of the modified polymer.[20] From the results it can be inferred that the presence of NMIC as pendent chain in C-NMIC forms co-valent cross linking between its chloride atoms and amino groups present on the chitosan polymer backbone. In addition the decrease in the C/N ratio suggests that C-NMIC cross linking occurred successfully on the addition of NMIC. Thus chitosan was chemically modified by the successful incorporation of NMIC as specified in Scheme 2.

Table 1 Elemental analysis of chitosan and C-NMIC

	Element (%)			
Sample	C	H	N	C/N
Chitosan	40.43	6.57	7.17	5.63
C-NMIC	40.22	5.71	7.62	5.27

3.2 Characterization studies

3.2.1 FTIR for DAEC, NMIC and C-NMIC. The FTIR spectra in Fig. 1(a), indicates the formation of DAEC by the observation of basic characteristic peaks at 1652 cm^{-1} corresponding to the C=O stretch of ester.[21,33] The peaks due to asymmetric deformation of N–CH_3 group and C–O asymmetric stretch of ester appeared at 1496 cm^{-1} and 1254 cm^{-1} respectively.[22,26] The presence of alcoholic OH confirms the successful cationization of DAEC by the appearance of peak at 3464 cm^{-1} (Fig. S1(b)†).[23] The peak at 602 was assigned to C–Cl stretching of the so formed CHPDAEC (NMIC).[21,24]

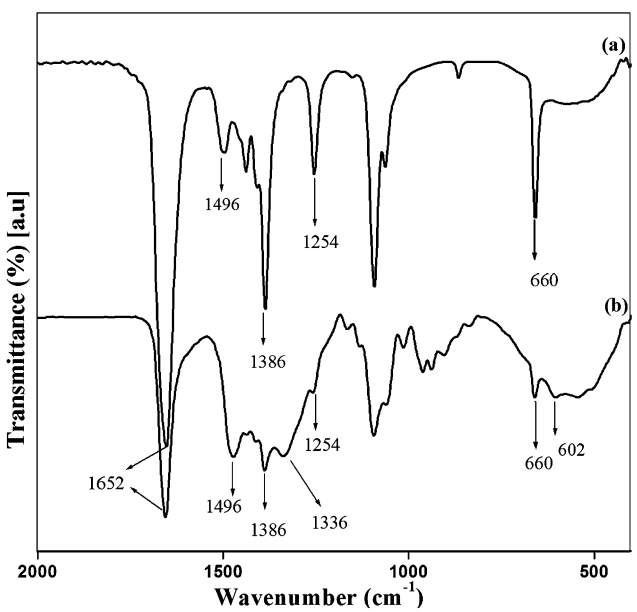

Fig. 1 FTIR spectra of (a) DAEC and (b) NMIC.

The unmodified chitosan spectrum (Fig. 2(a)) was similar to that of previously reported.[25–28] In comparison to the supporting biomaterial chitosan, the FTIR spectra (Fig. 2(b)) of the prepared C-NMIC confirmed the successful addition of NMIC to chitosan through N-linkage by the appearance of new peak at 1546 cm^{-1}.[28] It should be noted that unlike chitosan, a characteristic band could be observed at approximately 1470 cm^{-1} in the C-NMIC sample, which was a clear evidence for the chemical modification of chitosan.[25,29] Further, confirmation was done from the absence of peak at 602 cm^{-1}, that arose from C–Cl stretching of NMIC.[24]

3.2.2 NMR (^{1}H and ^{13}C) and mass spectroscopy. The ^{1}H-NMR spectrum as given in Fig. S3(a)† confirmed the formation of DAEC from the presence of characteristic resonances at 3.06 ppm and 3.91–3.95 ppm that were attributed to N–CH_3 (ref. 26) and O–CH_2 group protons respectively.[18,29–31] In Fig. S3(b),† the peaks at 3.4–3.48 ppm were assigned to CH_2–Cl protons[24] of NMIC that exhibited the neat cationization of DAEC with 1-chloro-2,3-epoxy propane.

As shown in Fig. S3(c),† ^{1}H-NMR of C-NMIC was similar to the one of chitosan except for the additional signals of N–CH_3, and (NH–CH_2) group protons at 3.3 ppm, 2.4–2.5 ppm respectively. These signals appeared as a singlet and doublet due to the presence of methyl and methylene protons.[18,26] The doublet at 2.4–2.5 ppm showed the N-crosslinking of original chitosan with NMIC. Since a pH of 7–8 was maintained, *N*-alkylation takes place predominantly leading to 80–90% N-crosslinked C-NMIC.[32]

The ^{13}C-NMR spectra (Fig. S4(a)†) indicated the formation of DAEC by the appearance of signals at δ_c 161, 67, 56 and 54 ppm for (*C*=O), (O–*C*H_2), (N–*C*H_2) and (N–*C*H_3) groups respectively.[18,32–34] In addition to the signals found in DAEC, resonances at δ_c 67 and 53 ppm for the newly formed NMIC were attributed to the methine carbon of *C*H–OH[32] and chloro carbon of *C*–Cl (Fig. S4(b)†).[24]

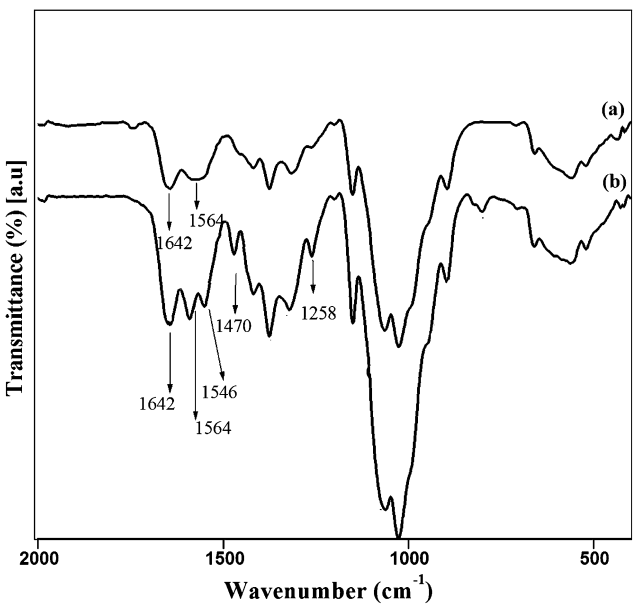

Fig. 2 FTIR spectra of (a) chitosan and (b) C-NMIC.

^{13}C-NMR spectra of C-NMIC exhibited the chitosan signals, that was consistent with that as reported earlier.[9,19,32] In addition signals at 167, 67, 61, 56, 54 and 52 ppm, were assigned to the NMIC carbonyl carbon, methine carbon of (*C*H–OH), methylene carbon of (O–*C*H_2), (N–*C*H_2), (NH–*C*H_2) and methyl carbon of (N–*C*H_3) respectively, which were an indication of neat formation of C-NIMC (Fig. S4(c)†).[19,31,32]

The EI mass spectra (Fig. S5(a) and (b)†) of the synthesized DAEC and NMIC showed molecular ion peak at (*m*/*z*) 207 and 391.2 respectively which was in good agreement with the calculated theoretical values.

3.2.3 X-ray diffraction (XRD) study for C-NMIC-Nps. The XRD profile of original chitosan and C-NMIC-Nps were given in Fig. S6(a).† The diffractograms of chitosan showed two peaks one at 2θ of 11.6° corresponding to anhydrous chitosan crystals and the other peak at 20.3° with (100) plane of orthorhombic crystals.[5] The diffractograms of C-NMIC-Nps (Fig. S6(b)†) showed large broad amorphous halo centred at $2\theta = 24°$ [4,39] that exhibits amorphous or disordered crystalline phase of chitosan. The decrease in chitosan crystallinity might be due to the weak ionic interaction of TPP which, diminishes the regularity of the extended C-NMIC crystal structure.[20,35] But, the results implied that the crystalline domains of chitosan were not disrupted completely due to the presence of the active and flexible NMIC groups present in C-NMIC-Nps.[7] The poly crystalline nature of the nanoparticles were further confirmed from the SAED pattern obtained from HRTEM analysis.

3.2.4 Thermo gravimetric analysis (TGA). The thermal stability of chitosan, C-NMIC and C-NMIC-Nps were studied by TGA analysis as shown in Fig. S7.† The initial weight loss of all the samples around 100 °C might be ascribed to the evaporation of absorbed water. It was noticed that the two TGA curves (a) and (b) showed similar trends at both low and high temperature. Rapid decomposition of the chitosan back bone occurred in the temperature range between 270 °C to 340 °C for both original chitosan and C-NMIC.[27,36,39] This indicated the good thermal stability of C-NMIC. TGA curve of C-NMIC-Nps curve (c) showed a lower shift in degradation temperature at 240 °C. This was mainly attributed to the ionic interaction of TPP with C-NMIC favouring the formation of nanoparticles.[28,36] The decrease in thermal stability confirmed the decrease in the crystalline nature of C-NMIC-Nps.[19]

From differential thermo gravimetric (DTG) curves (Fig. S8†), it was observed that the degradation temperature of chitosan in C-NMIC was lowered by 10 °C compared to original chitosan. This decreasing trend could be due to the random cross linking of NMIC having more number of polar groups with chitosan polymer backbone.[43] C-NMIC-Nps (Fig. S8(c)†) showed two decomposition peaks at 260 °C and 370 °C respectively. This corresponds to the degradation temperature of chitosan and TPP.[35] Once again herein, a further decrease in chitosan decomposition temperature would be due to the decrease in chitosan crystallinity that arises as a result of ionic cross linking of TPP with C-NMIC.[19] On the basis of the results obtained from TGA and DTG, it can be stated that increase of polar groups and decrease in the crystalline domains caused the reduction in thermal stability.

3.2.5 Particle size analysis using DLS, SEM and HRTEM analysis. The particle size data of C-NMIC-Nps by Dynamic light scattering (DLS) (Fig. 3(a)) showed a size range of 6.5 to 24 nm with a mean diameter of 14.4 ± 3.1 nm. SEM (Fig. 3(b)) and HRTEM (Fig. 3(c)) images showed that the average size of C-NMIC-Nps was around 10 nm with smooth surface and spherical morphology. The observed lattice fringes (Fig. 3(d)) with 3.8 Å inter lamellar spacing indicated that the crystalline structure was not destructed completely. Also, the selected area electron diffraction (SAED) pattern (Fig. 3(e)) of the nanoparticles supported the formation of polycrystalline C-NMIC nanoparticles.[4,37]

3.3 Biocompatibility study

Biocompatible studies were done to evaluate the suitability of any polymer based nanoparticles used for biomedical applications. Biocompatibility of the C-NMIC-Nps was carried out by MTT assay using VERO cell lines. Cell viability of VERO cells with different concentrations of pure C-NMIC-Nps along with control (100%) was assessed by MTT assay. MTT was used to assess the cell viability as a function of redox potential. Actively respiring cells convert the water soluble yellow tetrazolium MTT to an insoluble purple formazan.

It has been claimed that, the MTT formazan gives rise to extracellular deposits of needle-shaped crystals by exocytosis.[38] These crystals were dissolved in DMSO. The resulting purple solution was spectrophotometrically measured. The effect of the nanoparticles on the cell proliferation was expressed as (%) cell viability.[39–42]

The results (Fig. S9†) exposed that the C-NMIC-Nps at 0.5 mg mL^{-1} dilution after 72 h showed remarkable biocompatibility to VERO cell lines with a maximum cell viability of 93.5%. A slight decrease in cell viability was observed as the concentration of the C-NMIC-Nps increased from (0.5–2.5 mg mL^{-1}). This indicates the concentration dependent cytotoxicity of the nanoparticles.[43] The significant increase in the cell viability of C-NMIC-Nps at all given dilutions with increasing time interval (12 h to 72 h) suggested a good development of cells within. Thus the positive time dependence property was a neat indication of the cell adherence and proliferation over the C-NMIC-Nps. The phase-contrast images of the viable cells in VERO cell lines seeded on control and C-NMIC-Nps after 72 h of incubation were shown in Fig. S10.† The results suggested that the C-NMIC-Nps has negligible cytotoxicity. Hence, the nanoparticles were biocompatible with the living cells and act as a potential material for wound healing application.

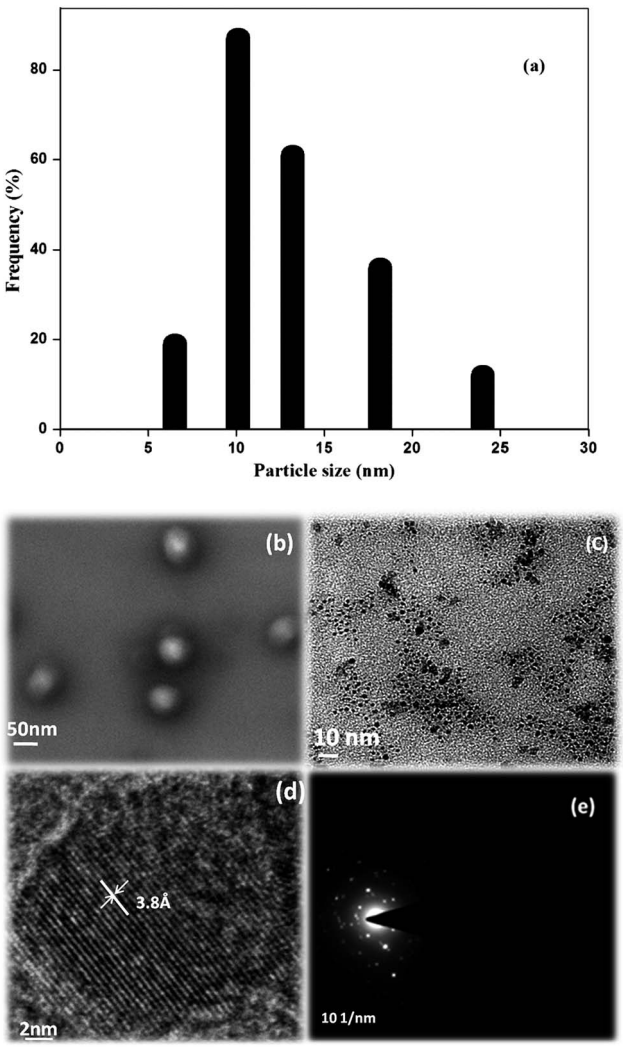

Fig. 3 (a) Particle size distribution obtained from DLS (b) SEM image (c) HRTEM image, (d) lattice fringes in HRTEM and (e) SAED pattern of C-NMIC-Nps.

4. Conclusion

In conclusion, synthesis of novel NMIC, preparation of C-NMIC and C-NMIC-Nps and their characterization has been reported. Cross linking of NMIC with biodegradable carbonate moiety through *N*-alkylation with chitosan was verified using instrumental analysis. The morphology of the nanoparticles as observed by SEM and TEM images were found to be smooth and spherical in shape. The size of the C-NMIC-Nps was found to be in 10 nm range. The C-NMIC-Nps were proved to be non-toxic and showed high cell viability 93.5% at a concentration of 0.5 mg mL^{-1} highlighting their potential application in biomedical field as growth factor nano carrier for wound healing application.

References

1 R. Riva, H. Ragelle, A. Rieux, N. Duhem, C. Jerome and V. Preat, *Adv. Polym. Sci.*, 2011, **244**, 19–44.
2 L. Qian and H. Zhang, *Green Chem.*, 2010, **12**, 1207–1214.
3 A.-H. Chen, S.-C. Liu, C.-Y. Chen and C.-Y. Chen, *J. Hazard. Mater.*, 2008, **154**, 184–191.
4 S. Sharma, P. Sanpui, A. Chattopadhyay and S. S. Ghosh, *RSC Adv.*, 2012, **2**, 5837–5843.
5 W. G. Malette, H. J. Quigley, R. D. Gaines, N. D. Johnson and W. Gerald Rainer, *Ann. Thorac. Surg.*, 1983, **36**, 55–58.
6 K. G. Desai and H. J. Park, *Drug delivery*, 2006, **13**, 375–381.
7 H. Xie, S. Zhang and S. Li, *Green Chem.*, 2006, **8**, 630–633.

8 H. Jonassen and A.-L. Kjøniksen, *Phys. Rev. E: Stat., Nonlinear, Soft Matter Phys.*, 2011, **84**, 1–4.
9 M. Bodnar, J. F. Hartmann and J. Borbely, *Biomacromolecules*, 2005, **6**, 2521–2527.
10 W. S. Wan Ngah, C. S. Endud and R. Mayanar, *React. Funct. Polym.*, 2002, **50**, 181–190.
11 H. Liu and C. Gao, *Polym. Adv. Technol.*, 2009, **20**, 613–619.
12 J. H. Park, G. Saravanakumar, K. Kim and I. C. Kwon, *Adv. Drug Delivery Rev.*, 2010, **62**, 28–41.
13 S. K. Samal, M. Dash, S. V. Vlierberghe, D. L. Kaplan, E. Chiellini, C. V. Blitterswijk, L. Moroni and P. Dubruel, *Chem. Soc. Rev.*, 2012, **41**, 7147–7194.
14 T. Dai, G. P. Tegos, M. Burkatovskaya, A. P. Castano and M. R. Hamblin, *Antimicrob. Agents Chemother.*, 2009, **53**, 393–400.
15 T. Dai, M. Tanaka, H. Ying-Ying and M. R. Hamblin, *Expert Rev. Anti-Infect. Ther.*, 2011, **9**(7), 857–879.
16 L. Zhao, B. Zhu, Y. Jia, W. Hou and C. Su, *BioMed Res. Int.*, 2013, **2013**, 1–7.
17 P. Tundo and M. Selva, *Acc. Chem. Res.*, 2002, **35**, 706–716.
18 F. Aricò, M. Chiurato, J. Peltier and P. Tundo, *Eur. J. Org. Chem.*, 2012, **17**, 3223–3228.
19 W. Sajomsang, S. Tantayanon, V. Tangpasthadol, M. Thatte and W. H. Daly, *Int. J. Biol. Macromol.*, 2008, **43**, 79–87.
20 E. C. N. Lopes, K. S. Sousa and C. Airoldi, *Thermochim. Acta*, 2009, **483**, 21–28.
21 K. S. Babu, M. S. Kumari, L. K. Ravindhranath and J. Latha, *Pharma Chem.*, 2013, **5**(5), 123–130.
22 M. M. J. Vijay Kumar, R. Yogananda, Snehalatha, H. Shameer, E. Jayachandran and G. M. Sreenivasa, *J. Biomed. Sci. Res.*, 2009, **1**(1), 1–10.
23 R. Jayakumar, R. L. Reis and J. F. Mano, *Drug Delivery*, 2007, **14**, 9–17.
24 D. Gor, P. Patel and P. S. Patel, *J. Curr. Chem. Pharm. Sci.*, 2012, **2**(4), 261–265.
25 H. S. Mansur, A. A. P. Mansur, E. Curti and M. V. De Almeida, *J. Mater. Chem. B*, 2013, **1**, 1696–1711.
26 P. D. Chethan, B. Vishalakshi, L. Sathish, K. Ananda and B. Poojary, *Int. J. Biol. Macromol.*, 2013, **59**, 158–164.
27 P. Kithva, L. Grøndahl, D. Martin and M. Trau, *J. Mater. Chem.*, 2010, **20**, 381–389.
28 C. L. Tien, M. Lacroix, P. Ispas-Szabo and M.-M. Mateescu, *J. Controlled Release*, 2003, **93**, 1–13.
29 W. Sajomsang, P. Gonil, S. Saesoo and C. Ovatlarnporn, *Int. J. Biol. Macromol.*, 2012, **50**, 263–269.
30 O. Kadkin, K. Osajda, P. Kaszynski and T. A. Barber, *J. Polym. Sci., Part A: Polym. Chem.*, 2003, **41**, 1114–1123.
31 M. Sobczak, C. Dębek, E. Olędzka, G. Nałęcz-Jawecki, W. L. Kołodziejski and M. Rajkiewicz, *J. Polym. Sci., Part A: Polym. Chem.*, 2012, **50**, 3904–3913.
32 W. Sajomsang, S. Tantayanon, V. Tangpasuthadol and W. H. Daly, *Carbohydr. Res.*, 2009, **344**, 2502–2511.
33 I. Kowalczyk, *Molecules*, 2008, **13**, 379–390.
34 S. Daoudi, A. A. Othman, T. Benaissa and Z. O. Kada, *Chem. Sci. Trans.*, 2014, **3**(1), 281–291.
35 D. R. Bhumkar and V. B. Pokharkar, *AAPS PharmSciTech*, 2006, **7**(2), 138–143.
36 Q. Chen, A. Xu, Z. Li, J. Wang and S. Zhang, *Green Chem.*, 2011, **13**, 3446–3452.
37 M. Li, Y. Wang, Q. Liu, Q. Li, Y. Cheng, Y. Zheng, T. Xi and S. Wei, *J. Mater. Chem. B*, 2013, **1**, 475–484.
38 Y. Liu, D. A. Peterson, H. Kimura and D. Schubert, *J. Neurochem.*, 1997, **69**, 581–593.
39 M. Liu, C. Wu, Y. Jiao, S. Xiong and C. Zhou, *J. Mater. Chem. B*, 2013, **1**, 2078–2089.
40 A. Cooper, N. Bhattarai, F. M. Kievit, M. Rossol and M. Zhang, *Phys. Chem. Chem. Phys.*, 2011, **13**, 9969–9972.
41 X. Zhong and F. Dehghani, *Green Chem.*, 2012, **14**, 2523–2533.
42 G. Millotti, C. Samberger, E. Fröhlich, D. Sakloetsakun and A. Bernkop-Schnürch, *J. Mater. Chem.*, 2010, **20**, 2432–2440.
43 N. S. Rejinold, M. Muthunarayanan, K. Muthuchelian, K. P. Chennazhi, S. V. Nair and R. Jayakumar, *Carbohydr. Polym.*, 2011, **84**, 407–416.

